Eur. Phys. J. D **28**, 163–170 (2004)
DOI: 10.1140/epjd/e2003-00298-x

THE EUROPEAN PHYSICAL JOURNAL D

The 1s → 2p resonance photoionization from the low-lying states of O^+

Energies, autoionization widths, branching ratios, and oscillator strengths

Jiaolong Zeng[1,2,a], Gang Zhao[1], and Jianmin Yuan[2]

[1] National Astronomical observatories, Chinese Academy of Sciences, 20A Datun Road, Chaoyang District, Beijing 100012, P.R. China
[2] Department of Applied Physics, National University of Defense Technology, Changsha 410073, P.R. China

Received 14 May 2003 / Received in final form 6 October 2003
Published online 2nd December 2003 –

Abstract. Thirty-state close-coupling calculations have been performed for the photoionization of O^+ near the $1s \rightarrow 2p$ resonance energy region from the terms belonging to the configurations of $1s^2 2s^2 2p^3$ and $1s^2 2s 2p^4$. Total and partial photoionization cross-section and the contributions of the main ionization channels to the partial cross-section are calculated to obtain the resonance energies, autoionization widths and Auger branching ratios of the $1s \rightarrow 2p$ core-excited states. The resonance oscillator strengths of the $1s \rightarrow 2p$ transitions are also obtained by integrating the photoionization cross-section. The radiative widths of the $1s \rightarrow 2p$ transitions can be obtained from the oscillator strengths. The results show that the radiative widths are generally three orders of magnitude smaller than the corresponding autoionization widths and therefore contributes little to the natural widths.

PACS. 32.80.Fb Photoionization of atoms and ions – 32.80.Hd Auger effect and inner-shell excitation or ionization – 32.80.Dz Autoionization

1 Introduction

Oxygen is an important element because of its existence in the earth′s atmosphere as well as in many astrophysical objects. For neutral oxygen atoms, there have been a few theoretical and experimental studies on the K-shell photoionization [1–5]. For oxygen ions of different ionization stages, most experimental and theoretical studies of the photoionization are in the photon energy range of vacuum ultraviolet, whereas investigations are very scarce on the inner-shell photoionization. Recently, we [6,7] considered the $1s \rightarrow 2p$ resonance photoionization of the doubly and triply ionized oxygen ions for the terms of $1s^2 2s^x 2p^y$ complex ($x + y = 4$ for O^{2+} and $x + y = 3$ for O^{3+}, $x = 2, 1, 0$). Most recently, the inner-shell photoionization for the ground term of O^{2+} was also calculated by Olalla et al. [8] and excellent agreement is found between the two theoretical oscillator strengths and autoionization widths. However, the study of photoionization in the inner-shell region is also very important, especially for X-ray astronomy and astrophysics. Recently, people have carried out some experimental studies on the inner-shell photoionization of atoms and ions in the soft X-ray region [9–12]. For the current status of the inner-shell spectroscopies of free atoms and molecules using high-resolution soft-X-ray monochromators installed in the soft-X-ray beamlines at the third-generation synchrotron radiation facilities, see a recent review article [9].

The valence-shell photoionization of O^+ has been investigated both theoretically [13–16] and experimentally [16,17]. Burke and Lennon [13] calculated the photoionization cross-section as part of the opacity project [18,19]. The opacity project used the close-coupling approximation implemented by the R-matrix method to calculate the energy levels, oscillator strengths and photoionization cross-sections. More recently the cross-sections were recalculated as part of the iron project [20] by Nahar [14,15], still using the R-matrix method but this time employing a larger basis set. Most recently, Covington et al. [16] have performed high-resolution absolute experimental measurements for the photoionization of O^+ ions from the $^2P^o$ and $^2D^o$ metastable states and from the $^4S^o$ ground state in the photon energy range 30−35.5 eV. Theoretical calculations have also been carried out to interpret the experiment and the result show that the cross-sections are sensitive to the choice of basis states. Kjeldsen et al. [17] have also measured the absolute photoionization cross-sections in region of 30−150 eV by merging a synchrotron-radiation beam from an undulator with a 2 keV ion beam.

[a] e-mail: zengjiaolong@sina.com

All of the above studies on the photoionization of O^+ were limited to the valence-shell energy region near the ionization threshold. There are few investigations which deal with the K-shell region near the $1s \rightarrow 2p$ autoionization resonances. Recently, Kawatsura et al. [12] measured the $1s \rightarrow 2p$ resonance photoionization in the energy range of 525−540 eV. This is the only experimental measurement on the $1s \rightarrow 2p$ resonance photoionization for O^+, as far as we know. There is no theoretical investigation, to the best of our knowledge, for the photoionization of O^+ near the $1s \rightarrow 2p$ region. However, the transition energies, oscillator strengths and autoionization widths of the $1s \rightarrow 2p$ resonances are important atomic data in dealing with the K-shell absorption or emission spectra. The $1s \rightarrow 2p$ transition from the atomic oxygen have been observed by the *Chandra X-ray Observatory* in the astrophysical objects [21]. There is also evidence that the $1s \rightarrow 2p$ absorption lines of O^+ exist in astrophysical objects [21,22]. The lack of accurate atomic data prevents the definite identification of these X-ray lines. There is obviously need to extend the photoionization of O^+ to the K-shell resonance region.

In the present study, close-coupling calculations are performed for the K-shell photoionization of the low-lying states of O^+ whose configurations belong to $1s^22s^22p^3$ and $1s^22s2p^4$ using the R-matrix method. The transition energies, oscillator strengths and autoionization widths of the $1s \rightarrow 2p$ resonances have been determined by analyzing the resonance structures of the cross-sections. Once an electron has been removed from an inner-shell subsequent electron cascades from higher shells of the ion will fill the vacancy. This process is accompanied either by a radiative transition or by a radiationless transfer of energy to an electron (Auger effect). As it will be demonstrated later that the Auger decay probability is far more larger than the radiative transition probability, the $1s \rightarrow 2p$ excited states tend strongly to decay to different ionic states. The Auger energies and branching ratios (BR) to the main decay channels for the Auger transitions are obtained from the calculation of photoionization as well. These data are very useful in interpreting and simulating the K-shell absorption or emission spectra for both astrophysical and laboratory plasmas. They are also helpful for analyzing the Auger spectra of O^+ ions.

2 Theoretical methods

The R-matrix method for electron-atom and photon-atom interactions has been discussed in great detail by Burke et al. [23]. The present calculations have been carried out by using the latest Belfast atomic R-matrix codes [24]. The R-matrix method is very effective in considering the resonance structures as shown in our previous papers [6,7,25–28]. We [29] simulated the X-ray transmission spectra through laser-produced aluminum plasmas (in the photon energy region of the $1s \rightarrow 2p$ resonances) using the R-matrix method. Good agreement is found between the experiment and theory with the autoionization widths having been considered in the calculation. In an R-matrix calculation, the wave function of the $N+1$ electron system is given the form

$$\Psi_k(X_1...X_{N+1}) = \hat{A}\sum_{ij} c_{ijk}\Phi_i(X_1...X_N\hat{\mathbf{r}}_{N+1}\sigma_{N+1}) \times u_{ij}(r_{N+1}) + \sum_j d_{jk}\phi_j(X_1...X_{N+1}) \quad (1)$$

where $\hat{A}$ is the antisymmetrization operator to take the exchange effect between the target electrons and the free electron into account. X_i stands for the spatial ($\mathbf{r}_i$) and the spin (σ_i) coordinates of the ith electron. The functions $u_{ij}(r)$ under the first sum construct the basis sets for the continuum wave functions of the free electron, and Φ_i are the coupling between the target states and the angular and spin part of the free electron. The correlation functions ϕ_j in the second sum are constructed by the square integrable orbitals to account for the correlation effects not adequately considered because of the cut-off in the first sum. The square integrable orbitals are cast as linear combinations of Slater-type orbitals

$$P_{nl} = \sum_j C_{jnl} r^{I_{jnl}} \exp(-\xi_{jnl} r). \quad (2)$$

The parameters ξ_{jnl} and coefficients C_{jnl} are determined by a variational optimization on the energy of a particular state, whilst the powers of r and I_{jnl} remain fixed. In the present calculation, thirteen orbitals ($1s$, $2s$, $2p$, $3s$, $3p$, $\overline{3d}$, $\overline{4s}$, $\overline{4p}$, $\overline{4d}$, $\overline{4f}$, $\overline{5s}$, $\overline{5p}$, $\overline{5d}$) are included in the expansion of the wavefunction of the target and $N+1$ electron systems. The bar on the orbital indicates that it is a pseudo-orbitals. The pertinent parameters ξ_{jnl} and coefficients C_{jnl} for all orbitals are obtained by using the CIV3 computer code [30] according to the following rules. The $1s$, $2s$ and $2p$ orbitals are taken from those of the Hartree-Fock orbitals given by Clementi and Roetti [31] for the O^{2+} ground state $2s^22p\ ^2P^o$, and the $3s$ and $3p$ orbitals are obtained by optimizing on the $2s^22p3s\ ^1P^o$ and $2s^22p3p\ ^3P$ states, respectively. The pseudo-orbitals $\overline{3d}$, $\overline{4s}$, $\overline{4p}$ and $\overline{4d}$ are obtained by optimizing on the $2s2p^3\ ^1D^o$, $2s2p^3\ ^1P^o$, $2s^22p^2\ ^1D$ and $2p^4\ ^3P$ states, respectively. The $\overline{4f}$, $\overline{5s}$, $\overline{5p}$ and $\overline{5d}$ orbitals are obtained by optimizing on the $1s$-hole states $1s2s^22p^3\ ^3D^o$, $1s2s2p^4\ ^3P$, $1s2s^22p^3\ ^3P^o$, and $1s2s2p^4\ ^3D$, respectively.

The appropriate R-matrix wave function expansion was performed by including 30 states of O^{2+} which are listed in Table 1, in which we also give the present calculated and experimental energy levels [32] relative to the ground state. Good agreement is obtained between the theory and experiment. R-matrix boundary was chosen to be 16 a.u. to ensure that the wavefunction is completely wrapped within the R-matrix sphere. For each angular momentum, the continuum orbitals are expressed as a linear combination of 50 numerical basis functions. In order to take account of the resonances of K-shell excited states, only one electron is fixed in the $1s$ orbital, at most two electrons can freely be excited among the included orbitals from the bases $1s^22s^22p^2$ and $1s^22s2p^3$ for the

Table 1. Theoretical and experimental energy levels [32] (in Ry) for the target O^{2+} ion relative to the ground state.

No.	State	Expt. [32]	Theory
1	$1s^2 2s^2 2p^2\ ^3P$	0.0	0.0
2	$1s^2 2s^2 2p^2\ ^1D$	0.18285	0.1861
3	$1s^2 2s^2 2p^2\ ^1S$	0.39164	0.4027
4	$1s^2 2s 2p^3\ ^5S^o$	0.54783	0.5379
5	$1s^2 2s 2p^3\ ^3D^o$	1.09200	1.0940
6	$1s^2 2s 2p^3\ ^3P^o$	1.29559	1.2959
7	$1s^2 2s 2p^3\ ^1D^o$	1.70267	1.7183
8	$1s^2 2s 2p^3\ ^3S^o$	1.79410	1.8072
9	$1s^2 2s 2p^3\ ^1P^o$	1.91598	1.9369
10	$1s^2 2s^2 2p 3s\ ^3P^o$	2.43591	2.4410
11	$1s^2 2s^2 2p 3s\ ^1P^o$	2.48661	2.4925
12	$1s^2 2p^4\ ^3P$	2.58489	2.5987
13	$1s^2 2s^2 2p 3p\ ^1P$	2.64951	2.6619
14	$1s^2 2s^2 2p 3p\ ^3D$	2.67795	2.6904
15	$1s^2 2s^2 2p 3p\ ^3S$	2.70966	2.7201
16	$1s^2 2p^4\ ^1D$	2.71636	2.7362
17	$1s^2 2s^2 2p 3p\ ^3P$	2.73534	2.7425
18	$1s^2 2s^2 2p 3p\ ^1D$	2.79192	2.8018
19	$1s^2 2s^2 2p 3p\ ^1S$	2.85769	2.8702
20	$1s^2 2p^4\ ^1S$	3.12654	3.1566
21	$1s 2s^2 2p^3\ ^5S^o$		38.660
22	$1s 2s^2 2p^3\ ^3D^o$		39.539
23	$1s 2s^2 2p^3\ ^3S^o$		39.606
24	$1s 2s^2 2p^3\ ^3P^o$		39.702
25	$1s 2s^2 2p^3\ ^1D^o$		39.798
26	$1s 2s^2 2p^3\ ^1P^o$		39.979
27	$1s 2s(^3S) 2p^4\ ^5P$		40.093
28	$1s 2s(^3S) 2p^4\ ^3P$		40.701
29	$1s 2s(^3S) 2p^4\ ^3D$		40.748
30	$1s 2s(^3S) 2p^4\ ^3S$		41.521

target states and from the bases $1s^2 2s^2 2p^3$ and $1s^2 2s 2p^4$ for the $N+1$ electron systems.

Once the photoionization cross-sections is obtained, the resonance oscillator strengths of the K-shell transition can be determined. It is well-known that the photoionization cross-sections can be written in terms of the differential oscillator strengths $df/d\epsilon$

$$\sigma = \frac{\pi h e^2}{mc}\frac{df}{d\epsilon} = 4\pi^2 \alpha a_0^2 \frac{df}{d\epsilon}, \tag{3}$$

where h is the Planck's constant, e the electron charge, m the electron rest mass, c the speed of light in vacuum, α and a_0 the fine structure constant and the Bohr radius, respectively. In the latter expression of equation (3), ϵ is in Ry. The resonance oscillator strengths can be obtained

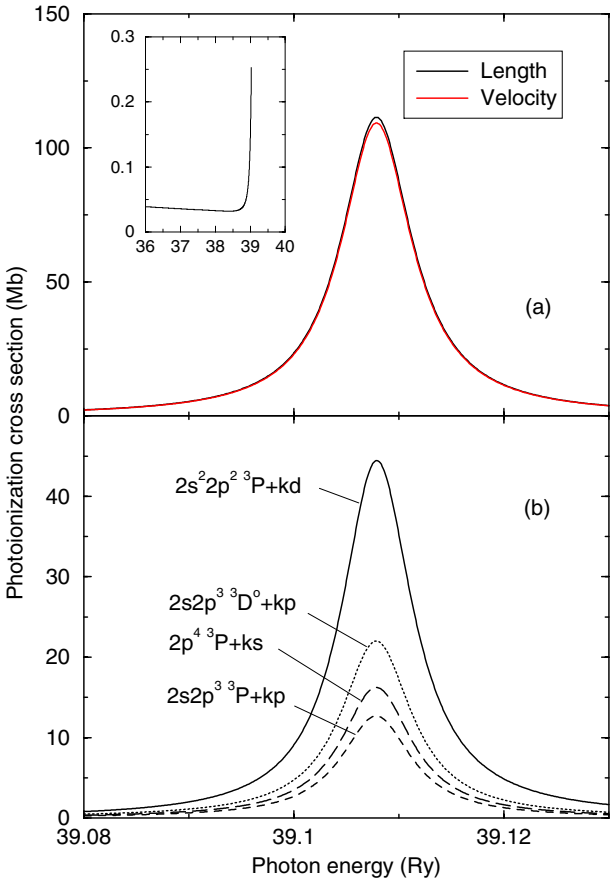

Fig. 1. (a) The photoionization cross-section of the ground state $1s^2 2s^2 2p^3\ ^4S^o$ of O^+ in the $1s \rightarrow 2p$ resonance region. The solid line refers to the length form and grayish line to the velocity form. The direct photoionization cross-section near the $1s \rightarrow 2p$ resonance is shown in the inset. (b) The contributions of the main ionization channels to the cross-section.

from the cross-sections σ

$$\overline{f}(L_i S_i \rightarrow L_j S_j) = \int_{\Delta E_r} \left(\frac{df(L_i S_i \rightarrow L_j S_j)}{d\epsilon}\right) d\epsilon = \left(\frac{1}{4\pi^2 \alpha a_0^2}\right) \int_{\Delta E_r} \sigma(\epsilon; L_i S_i \rightarrow L_j S_j) d\epsilon \tag{4}$$

where L_i, S_i, L_j, S_j are total spin and orbital angular momenta of the initial bound level and the final continuum wave function, respectively, governed by the dipole selection rules. The resonance oscillator strengths in length $\overline{f}_l$ and velocity $\overline{f}_v$ forms are determined from the corresponding (partial) photoionization cross-sections.

3 Results and discussion

Figure 1a shows the photoionization cross-section of the ground term $2s^2 2p^3\ ^4S^o$ of O^+ in the photon energy range of the $1s \rightarrow 2p$ resonance, with the solid line referring to

Table 2. Comparison of the calculated energies relative to the ground state $(1s^2)2s^22p^2\ ^3$P of the target O^{2+} with the NIST data (`http://physics.nist.gov/cgi-bin/AtData/main_asd`) (in Ry) for the low-lying terms of O^+.

Term	NIST	Theory	NIST-Theory	Diff. (%)
$2s^22p^3\ ^4$S^o	2.5832	2.5792	0.0040	0.15%
$2s^22p^3\ ^2$D^o	2.3389	2.3239	0.0150	0.64%
$2s^22p^3\ ^2$P^o	2.2145	2.1957	0.0188	0.85%
$2s2p^4\ ^4$P	1.4903	1.4806	0.0097	0.65%
$2s2p^4\ ^2$D	1.0706	1.0493	0.0213	1.99%
$2s2p^4\ ^2$S	0.7998	0.7691	0.0307	3.84%
$2s2p^4\ ^2$P	0.6454	0.6205	0.0249	3.86%

the length form and the grayish line to the velocity form. Excellent agreement is obtained between the two forms, the relative difference is less than 3.5% in the resonant energy region and less than 6% in the non-resonant region. Good agreement is also found for other terms, therefore, only length form is given for the other terms. It can be seen that a strong resonance superimposed on the very small direct photoionization cross-section. The direct photoionization cross-section in the vicinity of the $1s \rightarrow 2p$ resonance is shown in the inset. It is very small compared to that near the resonance. For example, it is only 0.035 Mb at a photon energy of 38.8 Ry, smaller than the cross-section at the peak (111.4 Mb at a photon energy of 39.1078 Ry) by more than three orders of magnitudes. The calculated ionization potential is 2.5792 Ry, in excellent agreement with the experimental value 2.5832 Ry [32]. The calculated values of ionization potential are listed in Table 2 along with the experimental values.

It is obviously that the resonance shown in Figure 1a should be identified as $1s2s^22p^4\ ^4$P. The photoionization cross-section carries information of position, autoionization width and oscillator strength of the $1s \rightarrow 2p$ resonance. The position and width can be obtained by fitting the resonance a modified Fano-Beutler profile [33] of the form

$$\sigma = \sigma_a + \sigma_b \frac{(q+\varepsilon)^2}{1+\varepsilon^2} \tag{5}$$

where σ_a and σ_b stand for constants related to the background of the resonance cross-sections, respectively, $\varepsilon = 2(E-E_0)/\Gamma$ with E being the photon energy, E_0 the resonance energy, Γ the resonance width and the parameters q describes the profile of the resonance. For the $1s2s^22p^4\ ^4$P resonance, the position and width are determined to be 39.1087 Ry = 532.093 eV and 0.0082 Ry = 111.6 meV, respectively. The resonance oscillator strength is determined from equation (4) to be 0.1702 and 0.1647 for the length and velocity forms, respectively. The positions, widths and oscillator strengths (in both length and velocity forms) are presented in Table 3. For convenience in astrophysical applications, the wavelength of the inner-shell transition is given as well. It is obtained from the following relation

$$\lambda(0.1\text{ nm}) = \frac{911.2341}{E(\text{Ry})}. \tag{6}$$

In the interstellar X-ray absorption spectroscopy of the low-mass X-ray binary X0614+091 observed by the *Chandra X-ray Observatory* [21], the authors concluded that the marginal evidence for a narrow absorption feature at ∼2.34 nm could be due to the absorption by ionized O, or O in molecules or dust. The position is very close to the wavelength 2.33 nm of the transition $1s^22s^22p^3\ ^4$S$^o \rightarrow 1s2s^22p^4\ ^4$P. To accurately identify the absorption features, one needs accurate atomic data such as wavelength, oscillator strength and natural width.

The $1s \rightarrow 2p$ inner-shell excited states are autoionized ones and tend to strongly decay to different ionic states. To determine the Auger branching ratios (BR), one needs partial cross-section and the contribution of the different ionization channels to the partial cross-section. Figure 1b shows the contribution of the main ionization channels to the cross-section of $1s^22s^22p^3\ ^4$S^o term. Four ionization channels ($1s^22s^22p^2\ ^3$P$+kd$, $1s^22s2p^3\ ^3$D^o+kp, $1s^22s2p^3\ ^3$P$^o + kp$ and $1s^22p^4\ ^3$P $+ ks$) contribute most to the $1s \rightarrow 2p$ resonance, whereas the $1s^22s^22p^2\ ^3$P $+ kd$ channel accounts for nearly 40%. The BR and Auger energies to the main decay channels are presented in Table 4. Note that some small BR which is less than 5% are not presented here, therefore, the sum of the given BR for a particular inner-shell excited states may not be necessarily equal to 100%.

From the inspection of Figure 1, one can see that the resonance profile is indeed asymmetric, yet it looks like a Lorentzian line shape. In the calculations, we have included the interchannel interactions among all the possible channels arising from the 30 target states listed in Table 1. To do this, in the expansion of the R-matrix wavefunction equation (1), we have considered all possible couplings among the target state Φ_i and the continuum orbital u_{ij}. The number of the u_{ij} (which is taken to be 50) is large enough to take all possible couplings into account. In general, the resonance line shape is asymmetric due to the interchannel interactions. This can easily be seen in the valence-shell photoionization [16,17] in the photon energy region 30−150 eV where the direct photoionization cross-section is large (>4 Mb in the present case). For example, in reference [16], some resonances shown in Figures 4, 6, and 7 show strong asymmetric. However, in the $1s \rightarrow 2p$ region, the direct photoionization cross-section (only 0.035 Mb at 38.8 Ry) is very small, therefore, the interactions between different decaying channels are also relatively small. On the other hand, qualitatively, the autoionization decay rate can be estimated by the coulomb interaction between the bound and continuum configurations of the two participating electrons. Among the four main decaying channels shown in Figure 1b, the radial part of the Coulomb matrix is rather small due to the quasi-orthogonality between the orbital functions except for the $1s^22s^22p^2\ ^3$P $+ kd$ channel. As a result, the $1s^22s^22p^2\ ^3$P$+kd$ channel is dominant (40%), the branching rations of other channels are <20%. Because the direct photoionization cross-section is very small, the line shape of this channel is rather symmetric. The other weak decaying channels are affected by the dominant channel and

Table 3. Resonance positions (E_r and λ), autoionization widths (Γ_a) and length ($\overline{f}_l$) and velocity ($\overline{f}_v$) forms of the oscillator strengths of the $1s-2p$ transitions for O^+.

Transition	E_r (Ry)	E_r (eV)	λ(0.1 nm)	Γ_a (Ry)	Γ_a (meV)	$\overline{f}_l$	$\overline{f}_v$
$1s^22s^22p^3\ ^4S^o$–$1s2s^22p^4\ ^4P$	39.1078	532.093	23.301	0.00820	111.6	0.1702	0.1647
$1s^22s^22p^3\ ^2D^o$–$1s2s^22p^4\ ^2D$	39.1628	532.841	23.268	0.00985	134.0	0.0871	0.0838
$1s^22s^22p^3\ ^2D^o$–$1s2s^22p^4\ ^2P$	39.1881	533.185	23.253	0.00754	102.6	0.0892	0.0860
$1s^22s^22p^3\ ^2P^o$–$1s2s^22p^4\ ^2D$	39.0345	531.096	23.344	0.00985	134.0	0.0485	0.0464
$1s^22s^22p^3\ ^2P^o$–$1s2s^22p^4\ ^2P$	39.0599	531.441	23.329	0.00754	102.6	0.0901	0.0857
$1s^22s^22p^3\ ^2P^o$–$1s2s^22p^4\ ^2S$	39.2447	533.956	23.219	0.00942	128.2	0.0381	0.0372
$1s^22s2p^4\ ^4P$–$1s2s2p^5\ ^4P^o$	39.1550	532.735	23.272	0.00682	92.7	0.1098	0.1072
$1s^22s2p^4\ ^2D$–$1s2s(^3S+^1S)2p^5\ ^2P$	39.1567	532.758	23.271	0.00923	125.6	0.1064	0.1021
$1s^22s2p^4\ ^2D$–$1s2s(^1S+^3S)2p^5\ ^2P$	39.5170	537.660	23.059	0.00923	125.6	0.0108	0.0105
$1s^22s2p^4\ ^2S$–$1s2s(^3S+^1S)2p^5\ ^2P$	38.8716	528.879	23.442	0.00923	125.6	0.1110	0.1056
$1s^22s2p^4\ ^2S$–$1s2s(^1S+^3S)2p^5\ ^2P$	39.2318	533.780	23.227	0.00923	125.6	0.0129	0.0124
$1s^22s2p^4\ ^2P$–$1s2s(^3S+^1S)2p^5\ ^2P$	38.7226	526.852	23.532	0.00923	125.6	0.0824	0.0792
$1s^22s2p^4\ ^2P$–$1s2s(^1S+^3S)2p^5\ ^2P$	39.0831	531.757	23.315	0.00923	125.6	0.0070	0.0067

Table 4. Auger energy ($E_{\rm Auger}$) (in Ry) and branching ratios (BR) to the main decay channels for the Auger transitions of O^+.

State	Channel	BR	$E_{\rm Auger}$ (Ry)
$1s2s^22p^4\ ^4P$	$1s^22s^22p^2\ ^3P+kd$	39.8%	36.5286
	$1s^22s2p^3\ ^3D^o+kp$	19.7%	35.4346
	$1s^22s2p^3\ ^3P^o+kp$	11.3%	35.2327
	$1s^22p^4\ ^3P+ks$	14.5%	33.9299
$1s2s^22p^4\ ^2D$	$1s^22s^22p^2\ ^1D+kd$	46.7%	36.6528
	$1s^22s^22p^2\ ^1S+kd$	6.7%	36.4362
	$1s^22s2p^3\ ^1D^o+kp$	15.1%	35.1206
	$1s^22p^4\ ^1D+ks$	13.3%	34.1027
$1s2s^22p^4\ ^2P$	$1s^22s^22p^2\ ^3P+ks$	6.6%	36.8642
	$1s^22s^22p^2\ ^3P+kd$	43.7%	36.8642
	$1s^22s2p^3\ ^1D^o+kp$	16.9%	35.1459
	$1s^22p^4\ ^3P+ks$	20.3%	34.2655
$1s2s^22p^4\ ^2S$	$1s^22s^22p^2\ ^1D+kd$	35.1%	36.8629
	$1s^22s^22p^2\ ^1S+ks$	19.9%	36.6463
	$1s^22s2p^3\ ^3P^o+kp$	7.4%	35.7531
	$1s^22s2p^3\ ^1P^o+kp$	19.9%	35.1121
	$1s^22p^4\ ^1S+ks$	13.9%	33.8924
$1s2s2p^5\ ^4P^o$	$1s^22s2p^3\ ^3D^o+kd$	64.0%	36.5804
	$1s^22s2p^3\ ^3P^o+ks$	9.6%	36.3785
	$1s^22s2p^3\ ^3P^o+kd$	22.6%	36.3785
$1s2s(^3S+^1S)2p^5\ ^2P^o$	$1s^22s2p^3\ ^3D^o+kd$	47.4%	36.9921
	$1s^22s2p^3\ ^3P^o+ks$	8.1%	36.7902
	$1s^22s2p^3\ ^3P^o+kd$	16.5%	36.7902
	$1s^22p^4\ ^3P+kp$	21.1%	35.4874
$1s2s(^1S+^3S)2p^5\ ^2P^o$	$1s^22s2p^3\ ^1D^o+kd$	43.1%	36.7281
	$1s^22s2p^3\ ^1P^o+ks$	7.7%	36.5095
	$1s^22s2p^3\ ^1P^o+kd$	15.8%	36.5095
	$1s^22p^4\ ^3P+kp$	7.3%	35.8477
	$1s^22p^4\ ^1D+kp$	16.8%	35.7102

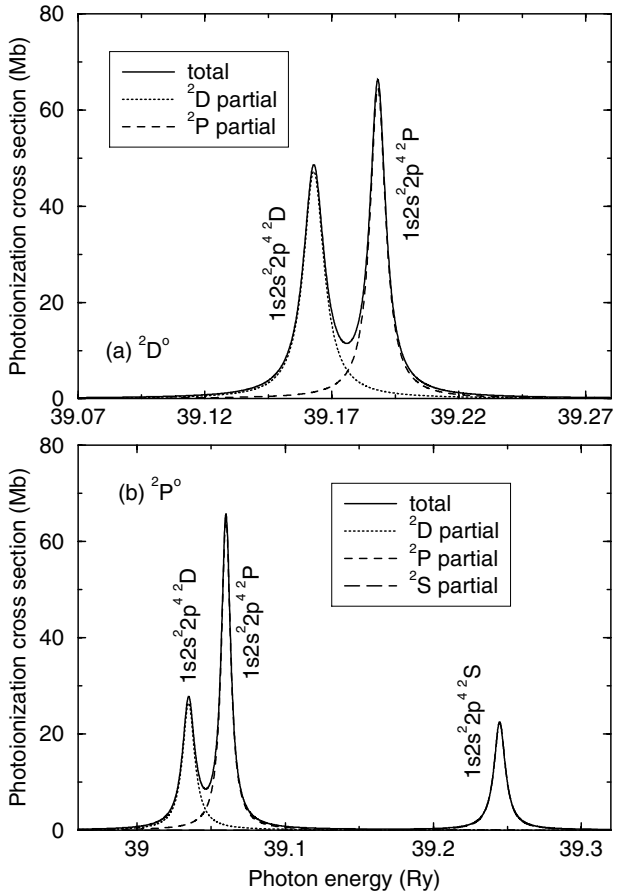

Fig. 2. The partial and total photoionization cross-sections of the metastable terms of (a) $1s^22s^22p^3$ ^{2}D° and (b) ^{2}P° in the vicinity of the $1s-2p$ resonances.

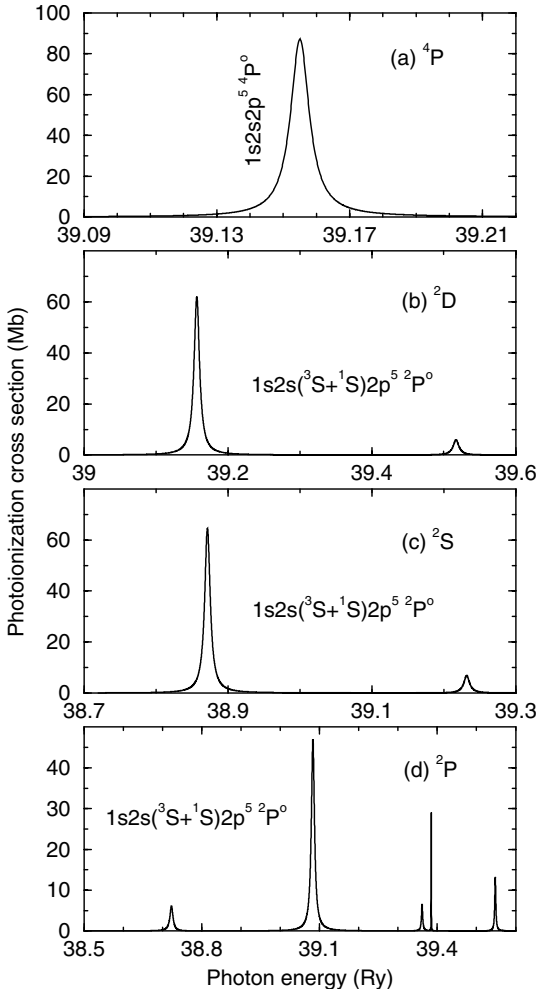

Fig. 3. The photoionization cross-sections of the terms: (a) ^{4}P, (b) ^{2}D, (c) ^{2}S and (d) ^{2}P for the configuration $1s^22s2p^4$.

thus they are more asymmetric than the dominant channel. However, the effects are not as prominent as in the valence-shell region.

Figure 2 gives the partial and total photoionization cross-section for the two metastable terms of (a) ^{2}D° and (b) ^{2}P° of the basic configuration $1s^22s^22p^3$. Figure 3 shows the total photoionization cross-section for the terms of (a) ^{4}P, (b) ^{2}D, (c) ^{2}S and (d) ^{2}P belonging to the first excited configuration $1s^22s2p^4$. For simplicity, the contributions of the main ionization channels to the partial cross-section are not given for the terms shown in Figures 2 and 3. The calculated values of ionization potential are listed in Table 2 for the terms mentioned above. It can easily be seen that good agreement is found between the experiment and theory for the ionization potentials of ^{2}D°, ^{2}P° and ^{4}P terms, the relative differences being <1%. While for the terms of ^{2}D, ^{2}S and ^{2}P, the relative differences are <4%. The positions, widths and oscillator strengths of the $1s \rightarrow 2p$ resonances are given in Table 3. The transition energies are around 530 eV and the autoionization widths range from 92.7 to 134.0 meV for the $1s \rightarrow 2p$ resonances. The average width is about 115 meV. In the experiment carried out by Kawatsura et al. [12], the authors determined the energy resolution power to be ∼310, which was estimated from the deconvolution of the measured spectra assuming a natural width of 140 meV, the same as the $1s$ natural width in oxygen atoms [2]. It is obviously that 140 meV is a little larger than the average autoionization width of 115 meV. On the other hand, the natural width is the sum of the autoionization and radiative widths. However, for the present case, the radiative width is much smaller than the autoionization width. The former can obtained from the transition probability

$$\Gamma_r(j) = \hbar \sum_i A_{ji} \tag{7}$$

where the summation is over all possible lower states. Take the $1s2s^22p^4$ ^{4}P as an example. The radiative width of this autoionized state is estimated to be about 0.5 meV, which is more than three orders of magnitude smaller than the autoionization width. Therefore, Kawatsura et al. [12] might have used a somewhat too large value than the natural width of O^+ ions. Finally, the Auger energies and branching ratios to the main decay channels are given in Table 4. There is one main decay channel for the core-excited states (but the BR is generally less than 50% for most cases), however, a few other channels have definite

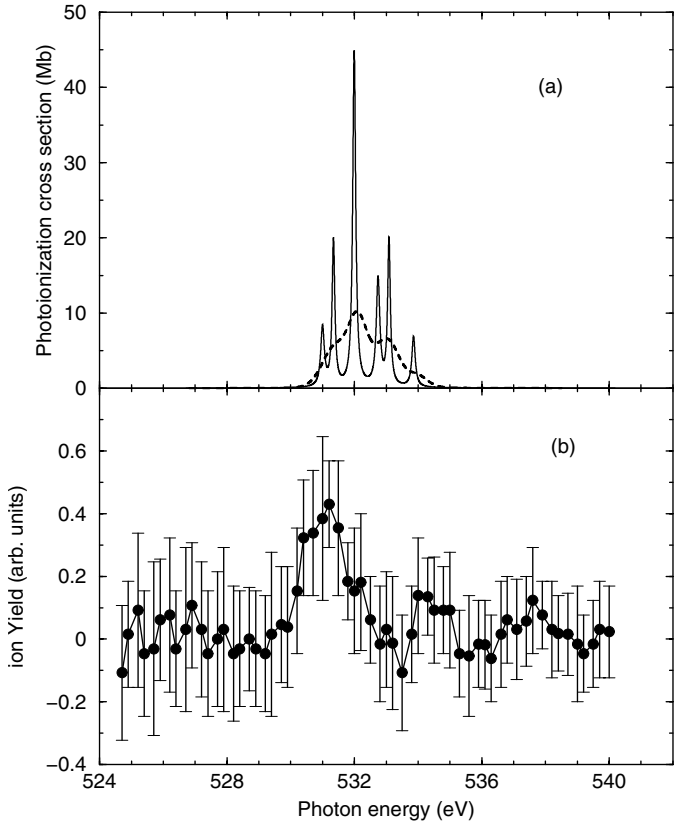

Fig. 4. (a) The photoionization cross-section for a mixture of 40% $2s^2 2p^3\ ^4S^o$, 30% $2s^2 2p^3\ ^2D^o$ and 30% $2s^2 2p^3\ ^2P^o$; (b) experimental spectrum carried out by Kawatsura et al. [12].

contributions. This is different from the case of Be-like neon [27], where most of $1s \rightarrow 2p$ excited states decay mainly via one channel.

In addition to the ground state, metastable states also exist in the experiment carried out by Kawatsura et al. [12]. This impurity may generally be a common feature in the experiments of photoionization for ions [16,17,34,35]. Covington et al. [16] even extracted the photoionization cross-section from the metastable states of O^+ near the photon energy of ionization threshold from the determined ion fraction. Unfortunately, Kawatsura et al. [12] did not report the fraction of the mixed terms in their experiment. Figure 4a gives, as an example, the photoionization cross-section for a mixture of 40% $1s^2 2s^2 2p^3\ ^4S^o$, 30% $1s^2 2s^2 2p^3\ ^2D^o$ and 30% $1s^2 2s^2 2p^3\ ^2P^o$. The solid line shows the result without consideration for the instrumental broadening, while the dashed line shows the result by convoluting the solid line with the experimental resolution. Figure 4b shows the experimental spectrum obtained by Kawatsura et al. [12]. As the fraction of ions is unknown in the experiment, quantitative comparison between the experiment and theory is not possible. But one can see that the overall structure is similar between the experiment and theory. One might also conclude that more initial terms exist in the experiment except for the terms included above. As mentioned by Kawatsura et al. [12], there is a need for additional experiment of high quality with higher photon-energy resolution and also better statistics to obtain the higher resolution spectra. Such data would be much more useful for astrophysical applications.

In conclusion, photoionization cross-sections from the low-lying terms belonging to the $1s^2 2s^x 2p^y$ complex ($x = 2, 1$ and $y = 3, 4$) of O^+ have been calculated in the photon energy range of $1s \rightarrow 2p$ resonances using the close-coupling R-matrix method. In general, the direct cross-section is more than three orders of magnitude smaller than that at the peak of the resonances. The resonance energies, autoionization widths and Auger branching ratios of the $1s \rightarrow 2p$ core-excited states have been obtained by analyzing the $1s \rightarrow 2p$ resonance structures. The resonance oscillator strengths of the $1s \rightarrow 2p$ transitions have been obtained by integrating the photoionization cross-section as well. These atomic data would be helpful in future experiments both on the photoionization and Auger spectra. The radiative widths of the $1s \rightarrow 2p$ transitions are much smaller than the autoionization widths and therefore its effects could be neglected.

We are very grateful to the anonymous referees for their helpful suggestions. This work was supported by the National Science Fund for Distinguished Young Scholars under Grant No. 10025416, the National Natural Science Foundation of China under Grant No. 10204024 and No. 19974075, the National High-Tech ICF Committee in China, and China Research Association of Atomic and Molecular Data. Jiaolong Zeng acknowledges the support from the CAS K.C. Wong Postdoctoral Research Award Fund.

References

1. H.P. Saha, Phys. Rev. A **49**, 894 (1994)
2. A. Menzel, S. Benzaid, M.O. Krause, C.D. Caldwell, Phys. Rev. A **54**, R991 (1996)
3. B.M. McLaughlin, K.P. Kirby, J. Phys. B **31**, 4991 (1998)
4. T.W. Gorczyca, B.M. McLaughlin, J. Phys. B **33**, L859 (2000)
5. W.C. Stolte, J.A.R. Samson, O. Hemmers, D. Hansen, S.B. Whitfield, D.W. Lindle J. Phys. B **30**, 4489 (1997)
6. Jiaolong Zeng, Jianmin Yuan, Qisheng Lu, J. Phys. B **34**, 2823 (2001)
7. Jiaolong Zeng, Jianmin Yuan, J. Phys. B **35**, 3041 (2002)
8. E. Olalla, N.J. Wilson, K.L. Bell, I. Martin, A. Hibbert, Mon. Not. R. Astron. Soc. **332**, 1005 (2002)
9. Kiyoshi Ueda, J. Phys. B **36**, R1 (2003)
10. M. Oura, H. Yamaoka, K. Kawatsura, J. Kimata, T. Haygaishi, T. Takahashi, T. Koizumi, T. Sekioka, M. Terasawa, Y. Itoh, Y. Awaya, A. Yokoya, A. Agui, A. Yoshigoe, Y. Saitoh, Phys. Rev. A **63**, 014704 (2001)
11. H. Yamaoka, M. Oura, K. Kawatsura, T. Sekioka, T. Agui, A. Yoshigoe, F. Koike, Phys. Rev. A **65**, 012709 (2002)
12. K. Kawatsura, H. Yamaoka, M. Oura, T. Hayaishi, T. Sekioka, T. Agui, A. Yoshigoe, F. Koike, J. Phys. B **35**, 4147 (2002)
13. Unpublished but the data are available through the TOPbase
14. S.N. Nahar, Astrophys. J. Suppl. Ser. **111**, 339 (1997)
15. S.N. Nahar, Phys. Rev. A **58**, 3766 (1998)

16. A.M. Covington, A. Aguilar, I.R. Covington, M.F. Gharaibeh, C.A. Shirley, R.A. Phaneuf, I. Alvarez, C. Cisneros, G. Hinojosa, J.D. Bozek, I. Dominguez, M.M. Sant'Anna, A.S. Schlachter, N. Berrah, S.N. Nahar, B.M. McLaughlin, Phys. Rev. Lett. **87**, 243002 (2001)
17. H. Kjeldsen, B. Kristensen, R.L. Brooks, F. Folkmann, H. Knudsen, T. Anderson, Astrophys. J. Suppl. Ser. **138**, 219 (2002)
18. M.J. Seaton, J. Phys. B **20**, 6363 (1987)
19. The Opacity Project team, *The Opacity Project* (Bristol, IOP Publishing, 1995), Vol. 1
20. D.G. Hummer, K.A. Berrington, W. Eissner, A.K. Pradhan, H.E. Saraph, J.A. Tully, Astron. Astrophys. **279**, 298 (1993)
21. F. Paerels, A.C. Brinkman, R.L.J. van der Meer, J.S. Kaastra, A.J.F. Den Boggende, P. Predehl, J.J. Drake, S.M. Kahn, D.W. Aavin, B.M. McLaughlin, Astrophys. J. **546**, 338 (2001)
22. K.C. Steenbrugge, J.S. Kaastra, C.P. de Vries, R. Edelson, Astron. Astrophys. **402**, 477 (2003)
23. P.G. Burke, A. Hibbert, W.D. Robb, J. Phys. B **4**, 153 (1971)
24. K.A. Berrington, W.B. Eissner, P.H. Norrington, Comput. Phys. Commun. **92**, 290 (1995)
25. Jiaolong Zeng, Jianmin Yuan, Qisheng Lu, Phys. Rev. A **62**, 022713 (2000)
26. Jiaolong Zeng, Jianmin Yuan, Qisheng Lu, Phys. Rev. A **64**, 042704 (2001)
27. Jiaolong Zeng, Jianmin Yuan, Phys. Rev. A **66**, 022715 (2002)
28. Jiaolong Zeng, Jianmin Yuan, Zengxiu Zhao, Qisheng Lu, Eur. Phys. J. D **11**, 167 (2000)
29. Jiaolong Zeng, Fengtao Jin, Jianmin Yuan, Qisheng Lu, Phys. Rev. E **62**, 7251 (2000)
30. A. Hibbert, Comput. Phys. Commun. **9**, 141 (1975)
31. E. Clementi, C. Roetti, At. Data Nucl. Data Tables **14**, 177 (1974)
32. NIST Atomic Spectra Data Base, `http://physics.nist.gov/cgi-bin/AtData/main_asd`
33. U. Fano, J.W. Cooper, Phys. Rev. A **137**, 1364 (1965)
34. A. Aguilar, J.B. West, R.A. Phaneuf, R.L. Brooks, F. Folkmann, H. Kjeldsen, J.D. Bozek, A.S. Schlachter, C. Cisneros, Phys. Rev. A **67**, 012701 (2003)
35. S. Schippers, A. Muller, S. Ricz, M.E. Bannister, G.H. Dunn, J. Bozek, A.S. Schlachter, G. Hinojosa, C. Cisneros, A. Aguilar, A.M. Covington, M.F. Gharaibeh, R.A. Phaneuf, Phys. Rev. Lett. **89**, 193002 (2002)